International Journal of Modern Manufacturing Technologies
ISSN 2067–3604, Vol. XIV, No. 2 / 2022
https://doi.org/ 10.54684/ijmmt.2022.14.2.96

INFLUENCE OF HEAT GENERATED IN A ROLLING BEARING ON ITS MOTION RESISTANCE

Jan Kosmol

Silesian University of Technology, Faculty of Mechanical Engineering, Department of Machine Technology
Konarskiego 18A, 44-100 Gliwice, Poland

Corresponding author: Jan Kosmol, jkosmol@polsl.pl

Abstract: The heat generated in a bearing may affect its resistance to motion. Therefore, the bearing seat designer should take this into account in the design process. The article presents the results of simulation tests which show how the heat in the bearing affects its resistance to motion. A methodology for determining the resistance to motion and power losses in the bearing has been proposed, which consists of two stages: identification of the temperature distribution in the bearing and identification of thermal deformation and contact loads. The main results of the research are the following statements: that the thermal deformation of the bearing elements is much greater than that due to mechanical loads (centrifugal forces or pre-load) and the contact loads, thus the motion resistance and power losses in the transient state may be much greater than in the state fixed. The conducted experimental studies show a relatively good qualitative agreement with the results of simulation tests, while the quantitative results do not always provide a sufficient agreement. The most important conclusion from the research is as follows: for high-speed assemblies, e.g. spindles of High Speed Cutting machine tools, the failure to take into account the motion resistance due to heat generated in the bearing may lead to a reduction in bearing life.

Key words: rolling bearing, heat, temperature, resistance to motion, power losses

1. INTRODUCTION

The development of HSC (High Speed Cutting) requires both proper cutting tools and machine tools. HSC machine tools are technological machines of considerably higher spindle rotational speeds and feed motion speeds, equipped with a servo system of significantly higher dynamic properties, i.e. allowing to obtain multiple times higher interpolated movement accelerations, and these machines are, finally, mechatronic objects of considerably better vibrostability.

A serious structural problem of such machine tools is their thermal resistance, understood as resisting thermal deformation of units and components, resulting from increasing heat in kinematic motion pairs (i.e. bearings, guides and integrated drives). Increase in kinematic parameters causes a proportional increase in heat amount and, in turn, causes thermal deformations. Natural cooling is insufficient in many cases. This is why the designer of - for instance - a spindle box in a HSC machine tool has to foresee the necessity to use forced heat removal, e.g. from spindle bearing seatings.

The first question that arises in the context of cooling system design is how much heat will be generated and where. Moreover, taking into consideration that HSC machine tools are often equipped with the so-called electrospindles, i.e. integrated main drives, then - apart from bearings as potential heat sources - the motors, closed in the spindle box, should be considered as well since they provide a much stronger heat source.

In rolling bearings, motion resistances - understood as torque occurring on the drive shaft M_f - result from the following:

- resistances due to friction that result from elements (balls) rolling on raceways, $M_{f(r)}$,
- resistances due to friction that result from the sliding effect, i.e. effect of sliding elements (balls) on raceways, $M_{f(s)}$,
- resistances due friction that result from the spinning effect, i.e. effect of rolling elements spinning around their own axis on raceways, $M_{f(sp)}$,
- resistances due to friction of rolling elements on lubricant or oil, i.e. the so-called resistances due to lubrication, M_v,
- other resistances like due to cages M_{other}.

The friction torque on the drive shaft is, therefore, the sum of:

$$M_f = M_1 + M_v + M_{other} \quad (1)$$

where: M_f - Bearing friction torque [Nmm], M_1 - Friction torque due to load (weighted sum of $M_{f(r)}$, $M_{f(s)}$, $M_{f(sp)}$) [Nmm], M_v - Friction torque due to lubrication [Nmm], M_{other} – other resistances like a bearing cage resistances [Nmm].

Motion resistances M_1 determined in this manner are transformed into heat and may be illustrated as follows [13]:

$$M_1 = f_1 F_\beta d_m$$
$$f_1 = z\left(\frac{F_s}{C_s}\right)^y \qquad (2)$$
$$F_\beta = 0{,}9F_a ctg\alpha - 0{,}1F_r$$

where: F_a, F_r - Axial and radial load [N], F_s - Bearing static equivalent load [N], C_s - Bearing basic static load rating [N], α - Contact angel [rad], d_m – Bearing pitch diameter [mm], z, y - Factors depending on the bearing structure and lubrication method.

On the other hand, the moment of resistance due to viscous friction M_v is determined according to the commonly used model [5]

$$M_v = 10^{-7} f_o (\nu_o n)^{2/3} d_m^3 \quad if \quad \nu_o n \geq 2000$$
$$M_v = 160 * 10^{-7} f_o d_m^3 \quad if \quad \nu_o n < 2000 \qquad (3)$$

where: n–rotatopnal speed [rpm], ν_o– wiscosity [cSt].

Kosmol [8], [9], [10] and many other authors prefer a different method of calculating the resistance to motion M_1 in a bearing due to the external load and dynamic internal loads. In their models, the resistance to motion inside the bearing is a function of the contact loads occurring between the balls and raceways and the conditions of mechanical friction (coefficient of friction). Therefore, the starting point for estimating the resistance to motion M_1 is the identification of the contact loads between the ball and the outer race Q_o and the inner race Q_i. In the literature, you can find a number of publications in which analytical relationships between these loads and dynamic loads due to the centrifugal forces, due to the spin phenomenon, due to the gyroscopic phenomenon and due to preload are shown.

In addition, the determination of the moment of resistance M_1 due to the above-mentioned loads requires their reduction to the drive shaft, which in turn requires a detailed kinematic analysis of the bearing. The author [8] presented a certain methodology for that.

The issue in itself is the thermal analysis of the bearing in the context of the power lost in the bearing and its influence on thermal deformation.

All publications available in the literature take into account the fact that the bearing is one of the heat sources in a complex mechanical system, e.g. in a machine tool spindle system. In this case, the bearings significantly affect thermal deformation in the mechanical system and, consequently, the geometric accuracy of e.g. machine tools.

Sum-Min & Sun-Kuy [14] present a simulation method to establish a comprehensive prediction model for the thermal and mechanical behavior of a spindle – bearing system in consideration of bearing surroundings such as assembly tolerance, geometric dimension, cooling conditions, operating conditions and thermal deformation. As a result of the research, they found that in the transition state, the contact pressure between the ball and raceways changes, which affects the resistance to motion in the bearing.

Muszynski at all [12] present a way of modeling the heat and temperature distribution on a test rig using the Finite Element Method. An extended bearing contact model was adopted to model the magnitude of the contact forces which motion resistance and power of the heat source were determined from. Correct determination of heat source power and convection coefficients is a key issue in temperature field modeling. The paper contains sample results of model and experimental research for preload of a selected values and various bearing speeds.

Holkup at all [6] present a Finite Element Method based thermo-mechanical model of spindles with rolling bearings. The heat generated in the bearings and the motor is transferred to the spindle structure, and causes thermal expansion of spindle parts. The thermo-mechanical spindle model predicts temperature distribution and thermal growth, as well as bearing stiffness and contact loads, under specified operating conditions. Transient changes in temperatures, deformations, viscosity of the lubricant, and bearing stiffness are considered in the solution. The predicted bearing properties are used to estimate the changes in the dynamic behavior of spindles.

Wang at all [15] present a dynamic thermal-mechanical model to investigate the thermal characteristics in a spindle-bearing system. In this model, transient thermal analysis, static structure analysis and calculation of the boundary conditions are conducted as a solution loop. The transient boundary conditions, such as bearing stiffness, bearing heat generation and thermal contact conductance are calculated with the appropriate formulas and solution methodology. The proposed model provides a practical method to improve the prediction accuracy. The heat power due to external load was computed using the Palmgren model (2).

Damian & Paleu [3] present a method for the computation of the power loss in angular contact ball bearings. Dynamic effects, generated at high-speed, are also included as centrifugal forces and gyroscopic moments, balls and cage interactions, ball and cage drag and churning in the lubricating bath oil.

De-xing at all [4] considering the centrifugal force, gyroscopic moment and thermal expansion, ball loads equilibrium model was first established to analyze the bearing loads in a high-speed spindle. The radial and axial heat transfer, especially the effect of structural

constraints on bearings temperature was well characterized as well as the bearing mounting arrangement, and then an enhanced node planning scheme was proposed. The numerical solution by Matlab was obtained. As a result, the bearing temperature rise can be better forecasted, which may be beneficial to improve bearing operating accuracy as well as bearing service life

Zivkovic at all [17] present a 3D FE thermal model, which was based on the thermo-mechanical bearing model and the numerical model of the spindle. Based on thermo-mechanical analysis of bearings with angular contact, generated heat and thermal contact resistance (TCR) are determined for each position of the ball. Bearings are divided into several zones based on the geometry of their cross-section. The aforementioned constraints have been applied to the 3D FEM model which allowed for establishing temperature field distribution, and spindle thermal balance. In order to prove the efficacy of the proposed model, experimental measurements of spindle and bearing temperatures were done by using thermocouples and thermal imager.

Zverev at all [18] have developed a beam element model of high-speed spindle units. The thermal model incorporates a model of heat generation in rolling bearings and models for estimation of temperature and temperature deformations. The simplified engineering method by Palmgren [13] model (2) was used to estimate frictional resistances. It is found out that the operation conditions make stronger effect on spindle unit temperatures when rotational speed increases.

The following conclusions can be drawn from the presented literature review:

1) Bearings are treated as significant heat sources, the power of which is estimated primarily based on the Palmgren [13] model (1) and (2) or less frequently based on the contact loads between the balls and raceways.

2) Few reports in the literature deal with the impact of thermal deformation of bearing elements on its motion resistance. This issue is the subject of research, the results of which are presented in this article.

2. FEM MODEL OF THE RESEARCH OBJECT

Due to the complexity of the problem, the Finite Element simulation method was used.

The object of the simulation tests is the test stand for measuring the resistance to motion of rolling bearings, which was established at the Department of Mechanical Engineering at the Silesian University of Technology [2]. From a structural point of view, the stand is similar to a classic machine headstock, i.e. it consists of a shaft (spindle) mounted on two preloaded angular contact bearings and a headstock body (Fig. 1a).

a)

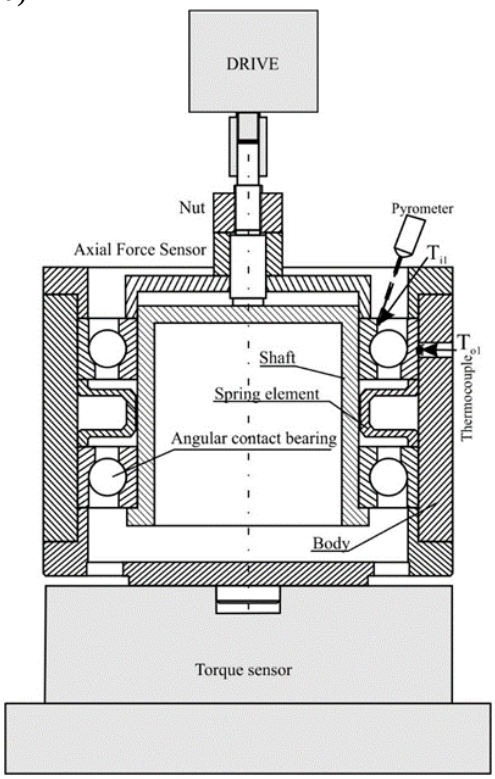

b)

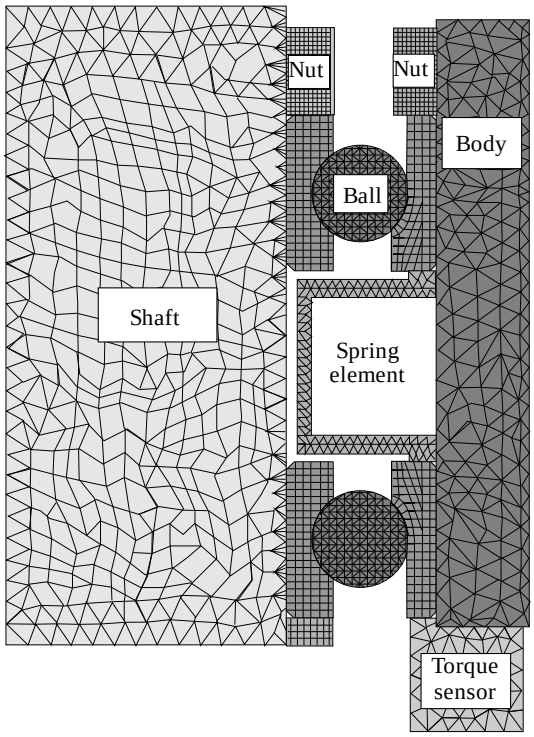

Fig. 1. Cross-section of the stand for measuring resistances to motion of rolling bearings (a) and its geometric model FEM (b): T_{o1}, T_{i1} – temperatures on the outer and inner rings of the bearing

On the other hand, Fig. 1b shows the geometric model of the object for the needs of FEM research. The FEM model is simplified in relation to the real object (Fig. 1a) because the axes of symmetry of the bearing were used. As a result, the FEM model is only 1/N of the entire bearing, where N - the number of balls in the bearing.

In the FEM model, the most important from the point of view of the research objective are the models of ball contact with raceways. It was assumed that, depending on the purpose of the research, these will be *Frictional* [16] models, which enable modeling of displacements and friction, or *Bonded* models. Chapter 3 explains when which models were used.

In the FEM model, there are also several other contact models, such as contacts of the bearing rings with the shaft and the body, contacts of the elastic element with the outer rings of the bearings, contacts of the nuts with the bearing rings and with the shaft and the body, and finally the contact between the body and the torque sensor. In these cases, a slightly simpler contact model in the form of *Frictionless* [16] was adopted, which allows for modeling displacements without friction, while the *Bonded* model was used to model the temperature distribution. This approach resulted from the desire to reduce the size of the model and the time of solving the task (despite this, in the case of *Transient Structural* analyzes, the time of a single analysis often reached 20 or more hours). The FEM model of the entire facility created in this way contained approx. 250 thousand elements and over 500 thousand knots.

It was assumed, based on the results of experimental tests, that a single analysis would cover the bearing operating time of approx. 1 hour. It was only after this time that the real object reached its thermal steady state.

It was assumed that only for the bearing rotational speed of 6000 rpm, full *Transient Thermal* and *Transient Structural* analyzes will be performed. For the remaining rotational speeds of the bearing, *Steady-State Thermal* and *Static Structure* analyzes were performed, i.e. static analyzes. The static analyzes carried out in this way provided test results for only one time point, corresponding to the time of 3200 seconds, thanks to which the overall time of the entire simulation tests was significantly shortened.

The tests were carried out for test angular contact rolling bearings type *FAG 70B13-E* in the rotational speed range, i.e. 1000 - 9000 rpm and for preload of 100N - 1000N, because the experimental tests were also carried out in this range of speed and preload.

The simulation and experimental tests were carried out for two bearing operating conditions:

- without the presence of grease,
- in the presence of grease.

The reason for this was the desire to distinguish the influence of mechanical friction resistances and viscous friction resistances on the bearing motion resistance, and thus on the thermal state of the bearings.

3. ESTIMATING THE POWER LOSS IN THE BEARING

Before starting the simulation tests, it is necessary to estimate the power losses in the bearing on the basis of analytical models. These losses will reflect the power of the heat sources in the bearing. As the temperature distribution in the first step of the simulation tests is not known yet, the forecasted temperatures should be used to estimate these losses, e.g. based on the guidelines of bearing manufacturers. In the next steps, it will be possible to use the results of the thermal simulation tests from the previous steps to more accurately estimate these losses. Thus, in an iterative way, it will be possible to estimate the power losses that better reflect the real power losses.

The power loss in a bearing is a function of its resistance to motion and speed. The resistance to motion in the bearing which will be included in the analysis consists of resistance M_1 and resistance M_v.

Other sources of resistance to motion M_{other} e.g. from the friction of the balls against the cage were not taken into account in this study.

Viscous resistances M_v are well recognized and the relationships (3) it is adequate enough.

The dependence (3) shows that the viscous resistances directly depend on the rotational speed and the viscosity of the lubricant, which viscosity is a function of temperature. Therefore, the knowledge of the lubricant temperature is necessary to estimate the viscous resistance.

The following model of lubricant viscosity is found in the literature [18]:

$$\nu(T) = \nu_{40}\left(\frac{40}{T}\right)^{m}$$

$$m = \frac{\ln\left(\frac{\nu_{100}}{\nu_{40}}\right)}{\ln\left(\frac{100}{40}\right)} \tag{4}$$

where: ν – viscosity of the grease [cSt], T – temperature of the grease [^{0}C], ν_{40}, ν_{100} – viscosity of the grease at temperatures of 40^{0}C and 100^{0}C [cSt] (grease manufacturers often provide in their catalogs the values of the viscosity of the grease at 40^{0}C and 100^{0}C).

It is slightly more difficult to estimate the resistance to motion M_1 of the bearings due to the mechanical friction of the balls against the raceways. The

Palmgren model (2) is commonly used in the literature [13].
The main advantage of the model (2) is its simplicity. On the other hand, the disadvantage is that the influence of dynamic effects in the bearing due to the rotation of the balls and bearing rings, e.g. the influence of centrifugal forces, is not explicitly taken into account.
Author [7], [11], [9], [8] but also many other authors [14], [12], [3], [4], [17] present dynamic models in which contact loads due to phenomena such as centrifugal forces from the rotation of the balls, moments of forces due to the gyroscopic phenomenon in angular contact bearings, moments of forces due to the spin phenomenon, i.e. the rotation of the balls around their axis perpendicular to the contact surface of the balls with the raceways, is a function of the rotational speed of the bearing and its preload.
Fig. 2a shows results of own research in the form of the influence of rotational speed and preload of the bearing on the sum of contact loads $Q_i + Q_o$ in the area of contact with the outer race Q_o and the inner race Q_i for the test angular contact bearing type *FAG 70B13-E*.

a)

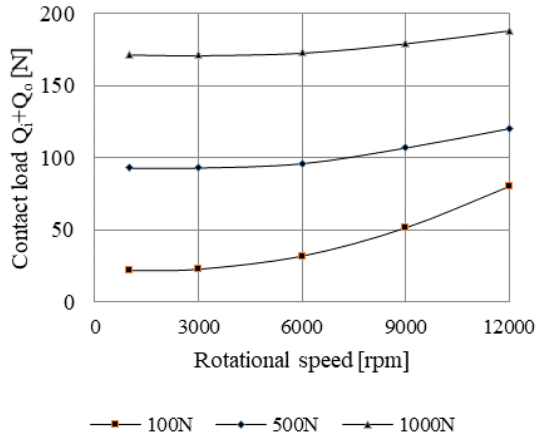

b)

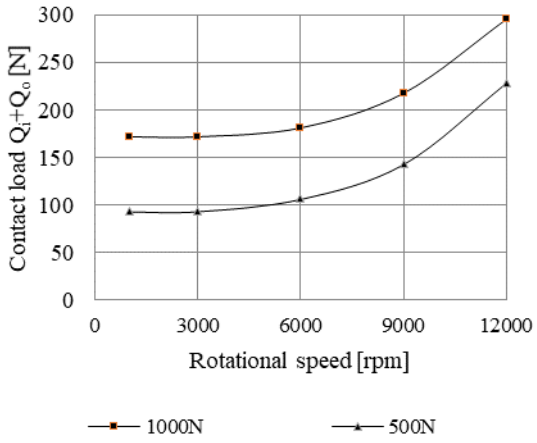

Fig. 2. Influence of the rotational speed of the ball (a) and the influence of the rotational speed of the ball and the inner bearing ring (b) on the sum of loads $Q_i + Q_o$ in the area of contact of the ball with the outer race Q_o and the inner race Q_i: 100N, 500N, 1000N - bearing preload

The increase in rotational speed and preload significantly influences the increase of contact forces (Fig. 2a) and hence the friction forces $(Q_i + Q_o)\mu$ (μ-coefficient of friction) and the resulting resistance to motion. According to the Palmgren model (2), the resistances due to velocity change do not change.
The author [11] also conducted research on the influence of the rotational movement of the bearing inner ring on contact loads, proposing the so-called extended model. This problem is rarely analyzed in the literature. Available publications [3], [17] on this topic contain assumptions with which the author does not agree.
Fig. 2b shows the results of such tests in the form of the sum of contact loads $Q_i + Q_o$ as a function of rotational speed and preload of the bearing. Even the visual comparative analysis of the results in Fig. 2a and Fig. 2b shows that taking into account the dynamic effects due to the rotational movement of the inner ring significantly increases the contact loads and thus the resistance to motion due to mechanical friction.
The author [8] showed how to calculate the moment of resistance measured on the bearing shaft on the basis of the contact forces Q_i and Q_o. The problem is quite complex because during the movement of the balls on the raceways, there is not only a rolling motion, but also a sliding motion and a spin motion. Each of these effects (rolling, sliding and spinning motion) has a different effect on the mechanical friction resistance of the balls against the raceways, but each can be expressed as a function of the contact loads Q_i and Q_o. Fig. 3 shows an example of the share of each of these effects on the total resistance to motion of the bearing.

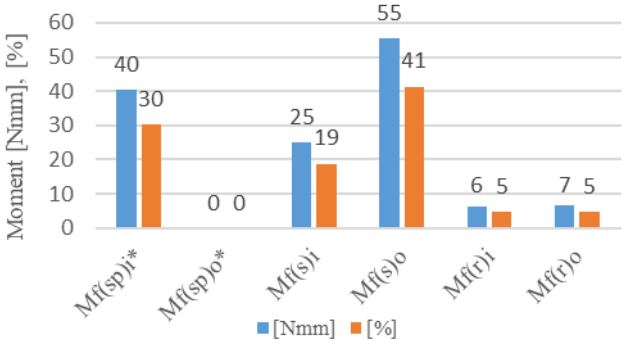

Fig. 3. Comparison of motion resistances in a bearing type *FAG 70B13-E* due to sliding $M_{f(s)i}$, $M_{f(s)o}$, spinning $M_{f(sp)i}{}^*$, $M_{f(sp)o}{}^*$ and rolling $M_{f(r)i}$, $M_{f(r)o}$ friction [8]

As can be seen, the share of slip resistance $M_{f(s)i}$, $M_{f(s)o}$ is the largest, over 50% of the total motion resistance, while the share of rolling resistance $M_{f(r)i}$, $M_{f(r)o}$ is the smallest.

Based on the analytical dependencies published, among others, in [7], [8], [9], the resistance to motion in bearings due to mechanical friction of balls against raceways was calculated. All the analytical relationships required knowledge of the contact loads Q_i and Q_o. In the literature, e.g. in [14], [12], [3], [4], [17] you can find the methodology for determining these loads. Also, the author in his publications, e.g. [7], [8], [9] presented analytical models that allow to calculate the values of contact loads.

Based on the moments of resistance, it is possible to determine the power losses in the bearing, which are the source of heat. For resistance to motion due to mechanical friction, the resulting power losses can be determined as follows:

$$\Sigma N_f = 10^{-3}\left(M_{f(s)o} + M_{f(s)i} + M^*_{f(sp)o} + M^*_{f(sp)i} + M_{f(r)o} + M_{f(r)i}\right)\omega \quad (5)$$

where: ΣN_f - power losses due to the mechanical friction of the balls against the raceways [W], $M_{f(s)i}$, $M_{f(s)o}$, $M_{f(r)i}$, $M_{f(r)o}$, $M^*_{f(sp)i}$, $M^*_{f(sp)o}$ - moments of resistance due to slip and ball rolling on raceways and due to the spin phenomenon ($M^*_{f(sp)i}$, $M^*_{f(sp)o}$) reduced to the drive shaft, on outer ($_o$) and inner ($_i$) rings [Nmm], ω - angular velocity of the shaft [s^{-1}].

In [8], the author presented detailed models that allow to calculate individual moments of resistance to motion in an angular contact bearing.

On the other hand, the loss of power due to viscous resistance can be determined as follows:

$$\Sigma N_v = 10^{-3} M_v \omega \quad (6)$$

where: ΣN_v – power losses due to viscosity [W].

Fig. 4a shows an example of the power losses $\Sigma N_f + \Sigma N_v$ in the test angular contact bearing for the forecast temperature and for the preload of the bearing 100N.

a)

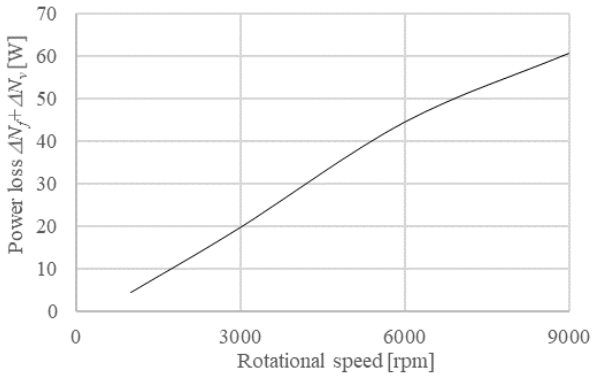

b)

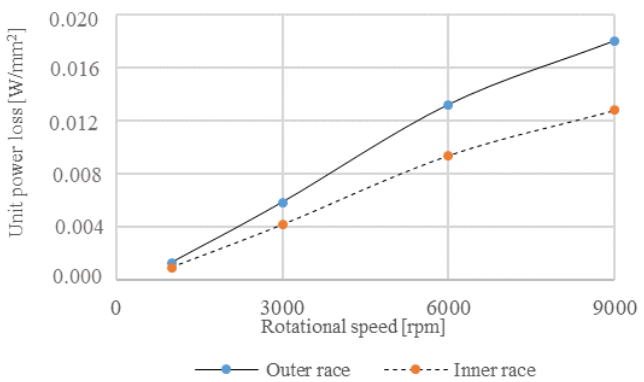

Fig. 4. Exemplary run of power losses $\Sigma N_f + \Sigma N_v$ as a function of rotational speed of the bearing (a), unit power losses on the outer and inner raceways (b)

Fig. 4a shows that the projected power losses in the test angular contact bearing, depending on the rotational speed, are within the range of 5 to 60 W. It has been assumed that all this power will be converted into heat, which arises due to the resistance to motion in the bearing.

The issue of quantifying the bearing power loss is not the only issue that needs to be solved before starting thermal simulation studies.

An equally complex issue is the arrangement of the heat sources in the bearing. There is no mention of this in the literature. The authors who conduct thermal tests of machines in which bearings are an important structural element, e.g. machine tools, do not provide detailed information on the methods of modeling heat sources in bearings. They are usually either point-located heat sources or by volume.

a) b) c)

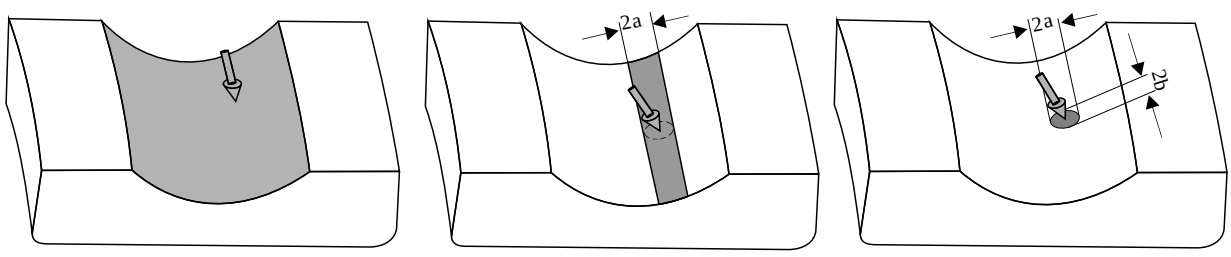

Fig. 5. Variants of modeling heat sources - heat sources assigned only to raceways [7]:

a,b - the semi-axes of the contact ellipse

The author [7] conducted extensive simulation studies on the influence of heat source modeling on the temperature distribution in the bearing. He took into account three ways of arranging heat sources in the bearing: on the full surfaces of the outer and inner raceways (Fig. 5a), on the sections of the outer and inner raceways (the section was a strip with the width of the longer semi-axis of the contact ellipse) (Fig. 5b) and on the area of the contact ellipse (contact surface of the ball with the raceway), Fig. 5c).

The conducted simulation studies [7] allow to formulate a conclusion that the method of distribution of heat sources has a small influence on the temperature distribution in the bearing, therefore the author suggests placing heat sources on the surface of the outer and inner raceways, which is the simplest from the technical point of view. On the other hand, quantitatively, the power losses (heat sources) assigned to the outer raceways ΣN_o and inner ΣN_i were determined as follows:

$$\begin{aligned} \Sigma N_o &= \Sigma N_{fo} + 0,5\Sigma N_v \\ \Sigma N_i &= \Sigma N_{fi} + 0,5\Sigma N_v \end{aligned} \tag{7}$$

where: ΣN_o, ΣN_i – power losses attributed to the outer and inner raceways [W], ΣN_{fo}, ΣN_{fi} – power losses due to mechanical friction attributed to the outer and inner raceways [W].

Dependence (7) shows that the power losses due to viscous resistance ΣN_v were allocated in 50% of the outer raceway and 50% of the inner race, while the power losses due to mechanical friction are proportional to the mechanical resistance occurring on these raceways,

The author also analyzed the impact of the ball-raceway contact model on the temperature distribution in the bearing, considering the models available in the Ansys R2020 software (*Bonded, Rough, Frictional, Frictionless, No separation*). The temperature differences in the bearing due to the adopted contact model exceeded 10^0C, i.e. they were very large.

The best agreement of the results of simulation tests of temperature distribution (*Transient Thermal* and *Steady-State Thermal*) and experimental tests (see Chapter 6) was obtained for the *Bonded* model. Therefore, in the simulation studies of the temperature distribution in the bearing, the *Bonded* model was used for the ball-raceway contact joints.

It should be noted that the best compliance of the simulation test results concerning, inter alia, thermal strains and contact loads (*Transient Structural* and *Static Structure*) with the experiment were obtained for the *Frictional* contact model.

The author also showed how the conditions of heat convection to the environment and heat conduction inside the bearing affect the temperature distribution in the bearing. The forced and free heat convection was estimated on the basis of the convection coefficients proposed by Buchmann&Jungnickel [1].

The designer of the bearing seat can significantly shape the temperature distribution inside the bearing by design (especially by selecting the surface that radiates heat to the environment). The author has shown by means of simulation studies that the forced emission of heat to the environment from the moving surfaces (surfaces of the moving inner ring of the bearing, balls and shaft) is much more intense than the free emission (from stationary surfaces, e.g. from the outer ring or seat body). Depending on the rotational speed of the bearing, the forced convection coefficient may be higher than the coefficient of free convection even 10 times.

Finally, for simulation purposes, the author calculated the unit power losses on the outer raceway ($\Delta N_o / A_o$) and the inner race ($\Delta N_i / A_i$) (Fig. 4b) based on the dependence (7) and the geometric surface of the outer raceway (A_o) and internal (A_i) as a function of rotational speed.

4. RESEARCH METHODOLOGY

As already mentioned, solving the problem requires iterative methods. Therefore, the test plan distinguishes two stages: the first is the identification of the temperature distribution in the bearing, and the second is the identification of thermal deformation and contact loads in the bearing.

In order to be able to implement the second stage, the first stage must be solved. But the solution of the first stage is possible only when the contact loads have been identified, i.e. when the second stage has been solved.

In accordance with the adopted test plan, in the first step, the influence of the bearing rotational speed and the resulting resistance to motion on the temperature distribution in the bearings and in the entire stand was estimated. This research was carried out in several steps. In the first of them, the power losses were estimated on the basis of analytical considerations presented in chapter 3.

It was assumed that in the first step, the temperature of the transition state viscosity in the bearing is unchanged and calculated (4) to equal the forecast temperature (the temperature suggested by the bearing manufacturer was adopted as the forecast temperature). For this viscosity, the viscous resistances (3) were calculated, which remained unchanged in the transition state. The mechanical friction resistances were determined on the basis of the methodology described in Chapter 3, without taking into account the influence of temperatures.

The dependence of the so estimated unit power losses assigned to the outer and inner raceways is shown in Fig. 4b.

Fig. 6 shows an example of the temperature distribution in the test stand, obtained from the *Transient Thermal* simulation tests for the speed of 6000 rpm. Fig. 7 shows the bearing transition temperature curves for 6000 rpm obtained from the *Transient Thermal* analysis. The run marked as "Temp_ v = const" applies to the first step of the simulation.

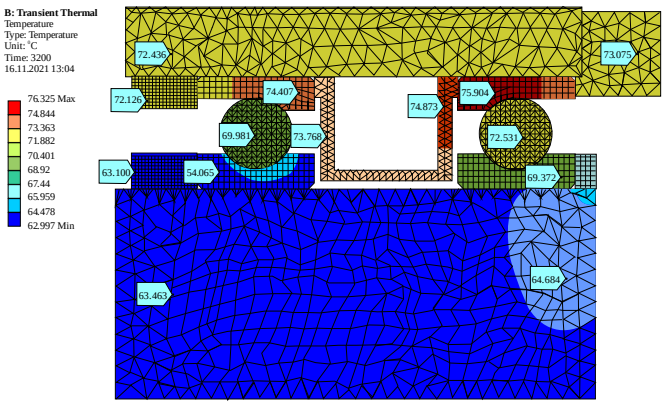

Fig. 6. An example of the temperature distribution in the test stand obtained from the *Transient Thermal* simulation tests for the speed of 6000 rpm

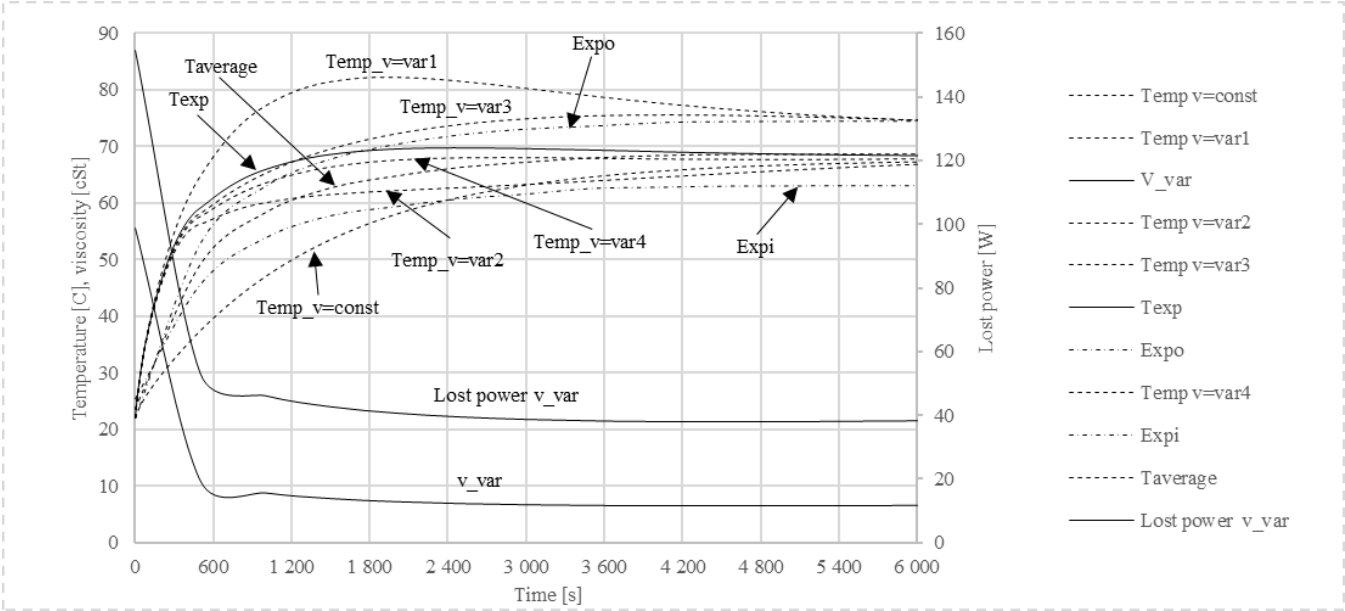

Fig. 7. Bearing temperature corses obtained from *Transient Thermal* analysis; Temp_v = const - temperature course for a constant viscosity of the grease, Temp_v = var1, Temp_v = var2,Temp_ v=var3, Temp_v=var4 – temperature courses for variable viscosity of the grease, v_var – viscosity course of the grease, Lost power v_var – lost power course, Expo, Expi – temperature courses on the outer and inner rings from experimental tests, Taverage – average temperature from Expo and Expi, Texp – temperature course from simulation tests for viscosity calculated on the basis of the average temperature course from experimental tests

Based on the course of temperatures in the first step "Temp_v = const", the course of viscosity v_var (dependence (4)) and the course of power losses due to viscosity change Lost power (dependence (6)) were determined.

In the second step, based on the power losses calculated in this way, the heat sources were modified in such a way that their power changed during the simulation, in line with temperature changes. The results of simulation tests for the thus calculated viscosity and viscous resistance are presented in the course marked as Temp_v=var1.

In the third step, the procedure from the second step was repeated with the only difference that the temperature course from the second step was used to calculate the viscosity and viscosity resistance. The simulation result in the third step shows the waveform marked as Temp_v = var2.

In step four, the procedure from step three was repeated, but the temperature course in step three was used to calculate the viscosity and viscosity resistance. The simulation result in step four shows the course marked as Temp_v = var3.

In step five, the procedure from step four was repeated, but the temperature course in step four was used to calculate the viscosity and viscosity resistance. The simulation result in step four shows the course marked as Temp_v = var4.

Fig. 7 also shows the temperature curves obtained from the experimental tests (see chapter 6) and marked as Expo (measured on the outer ring) and Expi (measured on the inner ring).

Comparative analysis of the simulated and experimental runs shows that after the fifth step the simulated run Temp_v = var4 and the averaged Taverage run between Expo and Expi are similar and that the temperature run after this step can be taken for further simulation tests.

Fig. 7 shows one more course of the simulated temperature, marked as Texp. It concerns the case for which the lubricant viscosity was calculated on the basis of the average Taverage temperature course obtained from experimental tests. It is also similar to the simulated run marked as Temp_v = var4.

Similar simulation tests were carried out for the bearing rotational speeds of 1000 - 3000 - 9000 rpm, and the obtained results are shown in Fig. 8.

The *To1*, *Ti1* and *To2*, *Ti2* temperatures were determined at the same points of the test stand as in the experimental tests (see Chapter 6).

As would be expected, the temperatures increase as the rotational speed increases. Due to the different conditions of heat dissipation in the test stand, the temperatures in bearing No. 1 and bearing No. 2 slightly differed.

Summarizing the first stage of the simulation tests, it can be stated that the obtained results of the tests Temp_v = var4 (Fig. 6) and those presented in Fig. 8 may constitute input data for the second stage of the tests, i.e. for simulation tests of thermal deformations and contact loads.

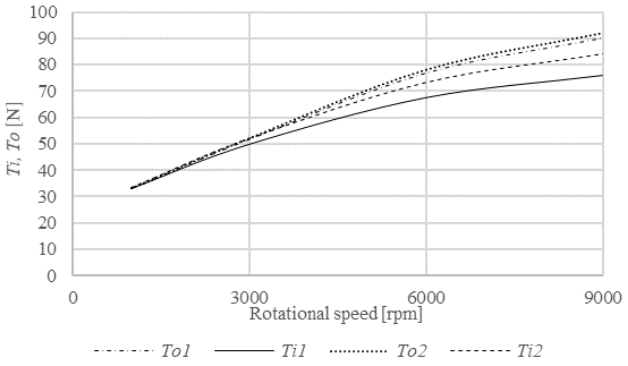

Fig. 8. The impact of rotational speed on bearing temperatures; *To1, Ti1* - temperatures on the outer and inner rings of bearing 1, *To2, Ti2* - temperatures on the outer and inner rings of bearing 2

The following analyzes were used to determine mechanical and thermal deformations as well as contact loads: dynamic (*Transient Structural)* and static (*Static Structure)*. The *Transient Structural* analysis allows you to track the deformation and contact load courses as a function of time, and the *Static Structure* analysis allows you to determine the deformation and contact loads at the end point of the simulation, i.e. after 3200 seconds. Due to the very long time of a single dynamic analysis, it was used only for one rotational speed, i.e. 6000 rpm, while for the remaining rotational speeds - the static analysis.

The most important advantage of these analyzes is the ability to import from *Transient Thermal* and *Steady-State Thermal* analyzes (*Imported Temperature*) and on their basis calculate thermal deformation and contact loads due to thermal deformation.

The study of deformations and contact loads was carried out both without taking into account thermal effects and with thermal effects. The literature presents only test results, analytical or simulation, without taking into account the thermal effects. Therefore, the results obtained in this study, without taking into account the thermal effects, can be compared to the results available in the literature. On the other hand, the author did not find the results of the research taking into account the thermal effects.

Conducting tests without taking into account thermal effects and with their participation allows for a quantitative assessment of the influence of temperature on deformations and contact loads in a rolling bearing.

In the *Transient Structural* and *Static Structure* analyzes it was assumed that the loads in the bearing come from the dynamic forces caused by the ball spinning around the bearing axis and the rotational movement of the inner ring (centrifugal forces), from static forces caused by the axial preload of angular contact bearings, from forces caused by thermal deformation of the elements bearings and the forces of viscous drag. The centrifugal forces were modeled by giving the balls the *Rotational velocity* ω_m (where ω_m is the speed of the bearing cage) and the inner ring rotational velocity ω (where ω is the bearing speed). The preload of two angular contact bearings was modeled by giving the shaft a preload deformation of *Bolt Pretension*, the size of which resulted from the expected axial preload force of both bearings and from the form stiffness of the elastic element placed between the two bearings. The forces of viscous resistance were modeled with the *Moment load*, by applying the load to the balls with the moment of force calculated according to (3). The contact connections of the balls with the raceways were modeled as *Frictional*, while the remaining contact connections, appearing in the construction of the test stand, as *Frictionless* or *Bonded*. In total, 19 contact connections were modeled in the FEM model of the test stand.

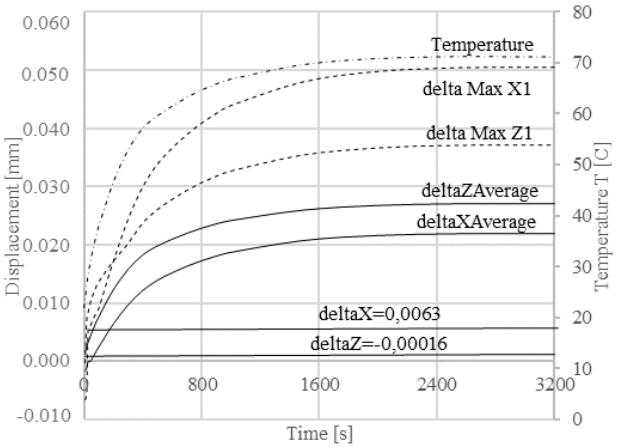

Fig. 9. An example of the course of deformations, i.e. average and maximum values in the X and Z axes under the conditions of mechanical and thermal loads, obtained from the *Transient Structural* analysis for the rotational speed of 6000 rpm; delta XAverage, delta ZAverage - average deformations in the bearing in the X and Z axes, delta MaxX1, delta MaxZ1 - maximum deformations in the bearing No. 1 in the X and Z axes, deltaX, deltaZ - maximum deformations without taking into account thermal deformations, Temperature - average temperature in bearing

Transient Structural and *Static Structure* analyzes enable the calculation of, among others form and contact deformations (*Total Deformation*) as well as their components (*Directional Deformation*) in individual axes of the XYZ coordinate system, contact loads in the form of a *Force Reaction* occurring between two contacting elements, e.g. between balls and raceways, in the form of reactions the resultant and its components in the XYZ axes and the reaction in the form of moments of force (*Moment Reaction*) occurring between two contacting elements, both the resultant and the individual components.

Fig. 9 shows an example of the deformation course, i.e. average and maximum values in the X and Z axes under the conditions of mechanical and thermal loads, obtained from the *Transient Structural* analysis for the rotational speed of 6000 rpm.

Fig. 9 also shows the maximum deformations in the X and Z axes (deltaX, deltaZ) without taking into account thermal deformations.

The first conclusion from these studies is obvious: an increase in temperature contributes to an increase in deformations, both in the X and Z axes. This conclusion applies to both average and maximum deformations.

The second conclusion is as follows: the thermal transition in the test stand lasts about 3200 seconds. After this time, both temperature and deformation do not change anymore.

The third and most important conclusion is as follows: deformations caused by the occurrence of mechanical and thermal loads are many times greater (even eight times) than the deformations caused by the occurrence of only mechanical loads (compare deltaMaxX1 to deltaX, and deltaMaxZ1 to deltaZ).

On the other hand, Fig. 10 shows an example of the course of the components of contact loads under the conditions of mechanical and thermal loads in the areas of contact of the ball with the outer (Q_o) and inner (Q_i) raceways in the X and Z axes.

The course marked with a dashed line relate to the *Transient Structural* analysis in the presence of mechanical loads (centrifugal forces, preload) and the *Imported Temperature* thermal loads, while the continuous lines denote contact loads corresponding to the occurrence of only mechanical loads (without thermal loads).

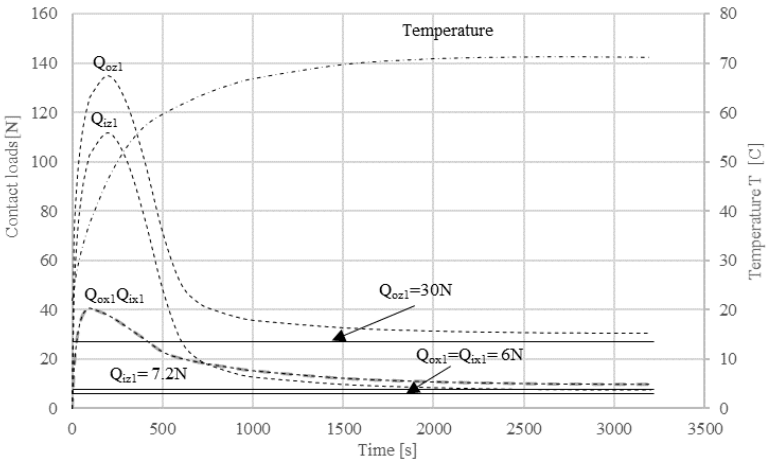

Fig. 10. An example of the course of the components of contact loads in the conditions of mechanical and thermal loads in the areas of contact of the ball with the outer (Q_o) and inner (Q_i) raceways in the X and Z axes; Q_{oz1}, Q_{ox1}, Q_{iz1}, Q_{ix1} - contact load components for bearing No. 1

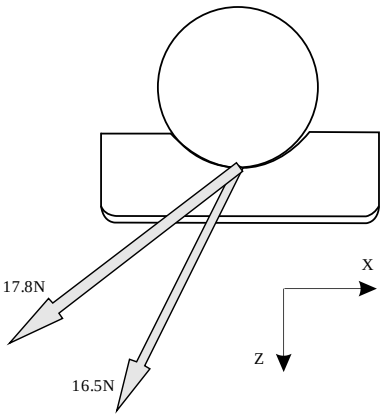

Fig. 11. Symbolic presentation of the vectors of contact forces Q_i: "17.8N" - including thermal effects, "16.5N" - without thermal effects

The course obtained from *Transient Structural* analysis are non-monotonic. In the first 100 seconds, we observe a dynamic increase in contact loads and then their decrease. This is mainly due to changes in the viscosity of the lubricant and, consequently, the viscous resistance caused by temperature changes in the bearings. After approx. 3200 seconds, the contact loads drop to the level at which they are, but without the participation of thermal loads, i.e. Q_{oz1} = 30N, Q_{iz1} = 7.2N, Q_{ox1} = 6N, Q_{ix1} = 6N.

It should also be noted that in the transient state, the maximum values of the component contact loads are approx. 4 - 5 times higher than in the steady state. This means that also the resistance to motion in the bearings in the transition state can change significantly. The mere fact of higher values of contact loads does not necessarily entail a proportional increase in motion resistance. Fig. 11 shows the comparative vectors of contact loads occurring on the inner raceway Q_i: 16.5N (without thermal effects) and 17.8N (taking into account thermal effects). Although the numerical values of these forces do not differ significantly, their directions of action differ. As the friction force is determined by the projection of the contact force onto the direction normal to the contact surface, the resistance to motion due to these contact forces will be varied. Important conclusions from such an analysis also include the observation that the values of the contact load components in the Z axis (Q_{oz1}, Q_{iz1}) are significantly higher than in the X axis (Q_{ox1}, Q_{ix1}), even 3-4 times.

In Ansys R2020, *Transient Structural* analysis can also calculate a moment as the reaction between two contact surfaces. As part of the research, the time course of the torque was simulated in the contact area of the body of the test stand with the torque sensor (Fig. 1a). An example of the torque curve, which is equivalent to the moment of resistance of two bearings on the test stand, is shown in Fig. 12.

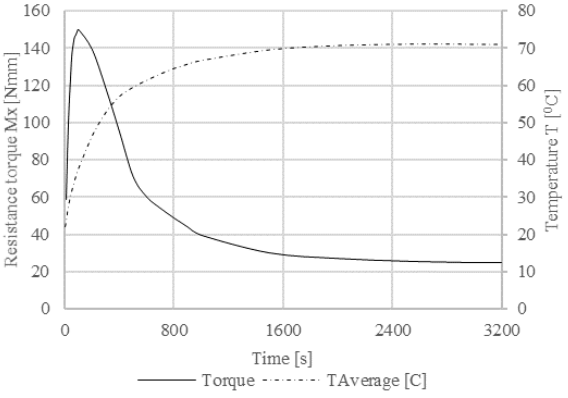

Fig. 12. An example of a torque curve obtained in the *Transient Structural* analysis with the participation of mechanical and thermal loads; TAverage [C] – average temperature

The course of this moment is similar to the courses of contact loads (Fig. 10), i.e. in the first period (up to approx. 100 seconds), the torque increases dynamically and then decreases relatively quickly to the set value. The maximum value of this moment in the transient state is approx. 6 times greater than the value in the steady state.

5. RESULTS AND DISSCUSIONS

The research methodology presented in chapter 4 was used for 1000 - 3000 and 9000 rpm, except that *Steady-State Thermal* and *Static Structural* were used instead of *Transient Thermal* and *Transient Structural* analyzes. The obtained test results regarding contact deformations, contact angles and contact loads are presented in Fig. 13. They concern the steady state after 3200 seconds.

The test results presented in Fig. 13a), c), e), g) concern the influence of mechanical loads (from centrifugal forces and preload, without the effects of thermal deformation), while those presented in Fig. 13b), d), f), h) relate to mechanical loads and the effects of thermal deformation.

When formulating conclusions, attention should be paid to the adopted coordinate system (Fig. 1b).

The results in Fig. 13a) and Fig. 13b) concern contact deformations in the contact area of the ball with raceways. The comparison of both results shows how significant is the influence of thermal phenomena in the bearing on contact deformation. The deformations in Fig. 13b) in the Z direction are over 10 times greater than in Fig. 13a) and in the X direction approx. 4-5 times greater. Moreover, the directions of the contact strains are opposite, i.e. in Fig. 13a) we can talk about a positive strain increment and in Fig. 13b) - a negative one. Fig. 13a) and Fig. 13b) also show total contact deformations δ_o, δ_i. They generally increase non-linearly with increasing speed. In Fig. 13b) they are approx. 5-6 times larger than in Fig. 13a). According to Hertz's theory, these deformations are functionally related to contact loads. The mere fact of greater contact deformation does not indicate greater resistance to movement, because the resistance to motion depends on the clearance between the ball and raceways. After preload of the bearings, the clearance is negative and its size depends on the mounting load of the bearings. The appearance of, for example, centrifugal forces or thermal deformations of bearing elements changes the value of the clearance, and this change may cause an increase or reduction of the previous negative clearance, and in extreme cases even the creation of a positive clearance. Therefore, Fig. 13c) and Fig. 13d) show the differences in contact deformations between the outer and inner raceways in the Z and X directions, δ_{ox} - δ_{ix} and δ_{oz} - δ_{iz}. These differences

better reflect the effect of contact deformation on the change in clearance between the ball and the raceways. One can speak of a monotonic increase in contact deformation differences with increasing speed. Moreover, differences in contact deformations caused by thermal effects (Fig. 13d), especially in the Z direction, are much greater than in Fig. 13c (without taking into account the thermal effects), approx. 10 times.

It should also be noted that the deformation differences in the direction Z (δ_{oz} - δ_{iz}) are of opposite signs, i.e. in Fig. 13c) they are positive and in Fig. 13d) they are negative. A positive difference in strains in the Z direction indicates that the outer and inner raceways are getting closer to each other, while a positive difference in strains in the X direction indicates that the outer and inner raceways are moving away from each other.

These figures also show the differences in total deformations δ_o - δ_i. They better reflect the state of play between the ball and the raceways. Although they (δ_o, δ_i) are not collinear, they speak of the approaching or receding of the outer and inner raceways.

The contact angles α_o, α_i play an important role in the analysis of contact loads Q_o, Q_i. In general, for analytical methods of solving contact problems, the contact angles must first be determined, followed by the contact loads.

Fig. 13e) and Fig. 13f) show the dependence of the contact angles on speed. The characteristics in Fig. 13e) are consistent with those found in the literature because there are no solutions in the literature that would take into account the influence of thermal effects.

In contrast, the characteristics in Fig. 13f) have the characteristics of originality, as they show the influence of thermal effects.

a)

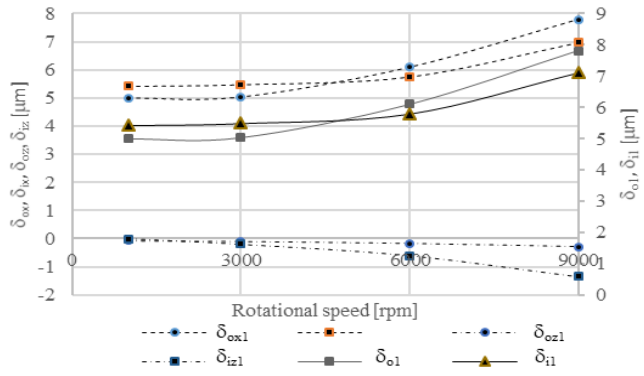

b)

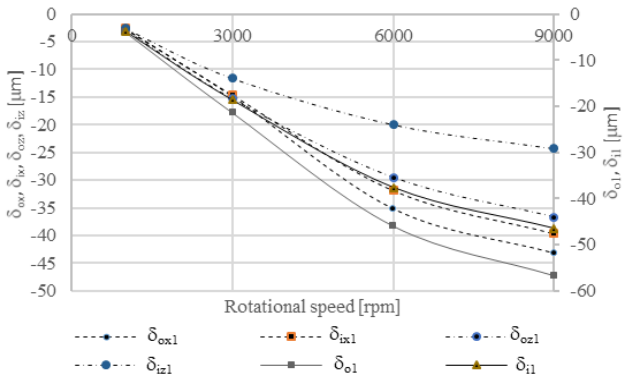

c)

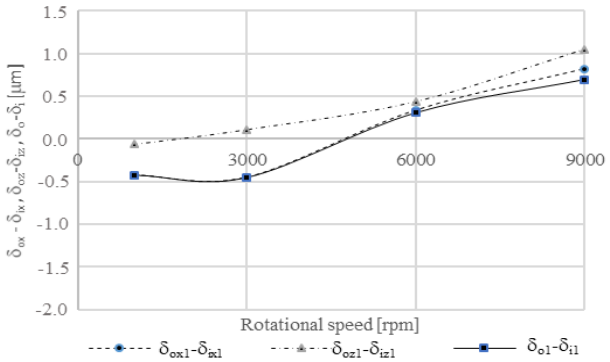

d)

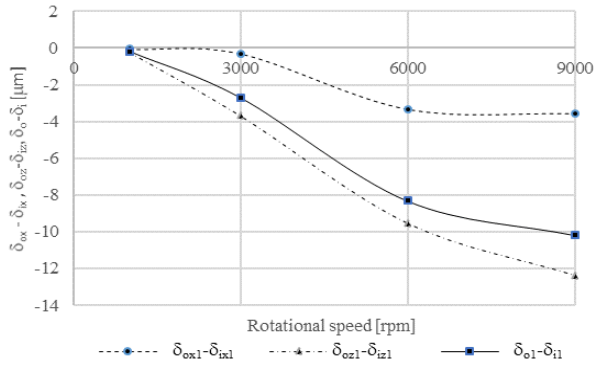

e)

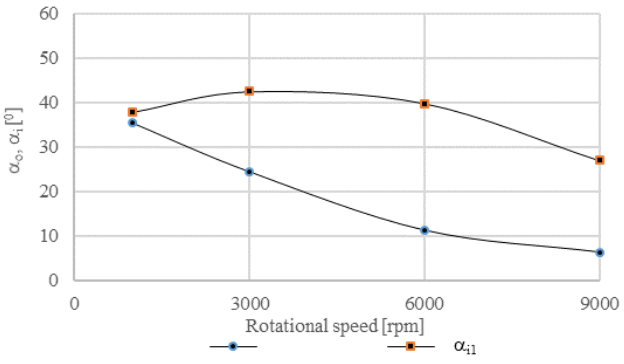

f)

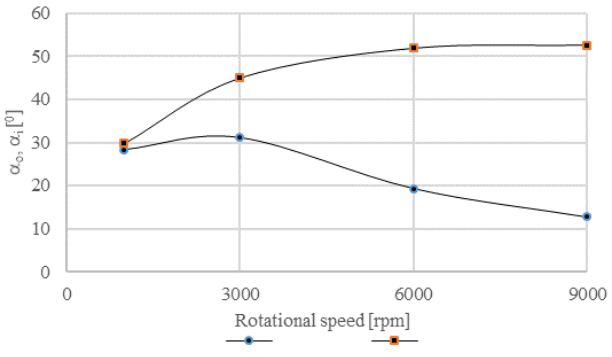

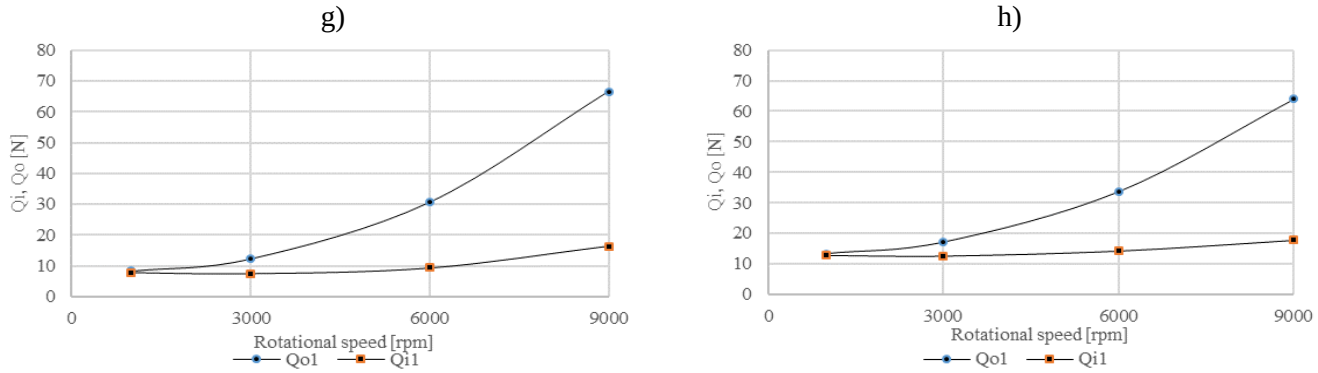

Fig. 13. The influence of rotational speed on: a), b) contact deformations, c), d) differences in contact deformations, e), f) contact angles, g), h) contact loads in the steady state, after 3200 seconds; δ_{ox}, δ_{ix} - contact deformations in the X axis, δ_{oz}, δ_{iz} - contact deformations in the Z axis, δ_o, δ_i - total contact deformations, Q_o, Q_i - contact loads, α_o, α_i - contact angles, $(_o)$ - ball - outer race contact area, $(_i)$ - ball - inner race contact area,
a), c), e), g) – for mechanical loads only, b), d), f), h) – for mechanical and thermal loads

The most important differences between the characteristics in Fig. 13e) and Fig. 13f) concern the contact angle α_i. In Fig. 13e) this angle decreases with increasing speed, and in Fig. 13f) it increases. The operating angles α_o in both figures show a decreasing tendency with increasing speed, although these characteristics are slightly different.

Fig. 13g) and Fig. 13h) show the effect of velocity on the contact loads Q_o, Q_i. The conclusion from the comparison of the two figures seems to be somewhat surprising: the thermal effects in the bearing do not significantly affect the contact loads, because the contact forces on both of them are very similar.

The differences do not exceed 10%. Note that this conclusion is for a steady state, 3200 seconds in this example. On the other hand, from the examples in Fig. 10, it can be concluded that if the operation time is shorter than 1000 seconds, the contact loads will be much greater than in the steady state.

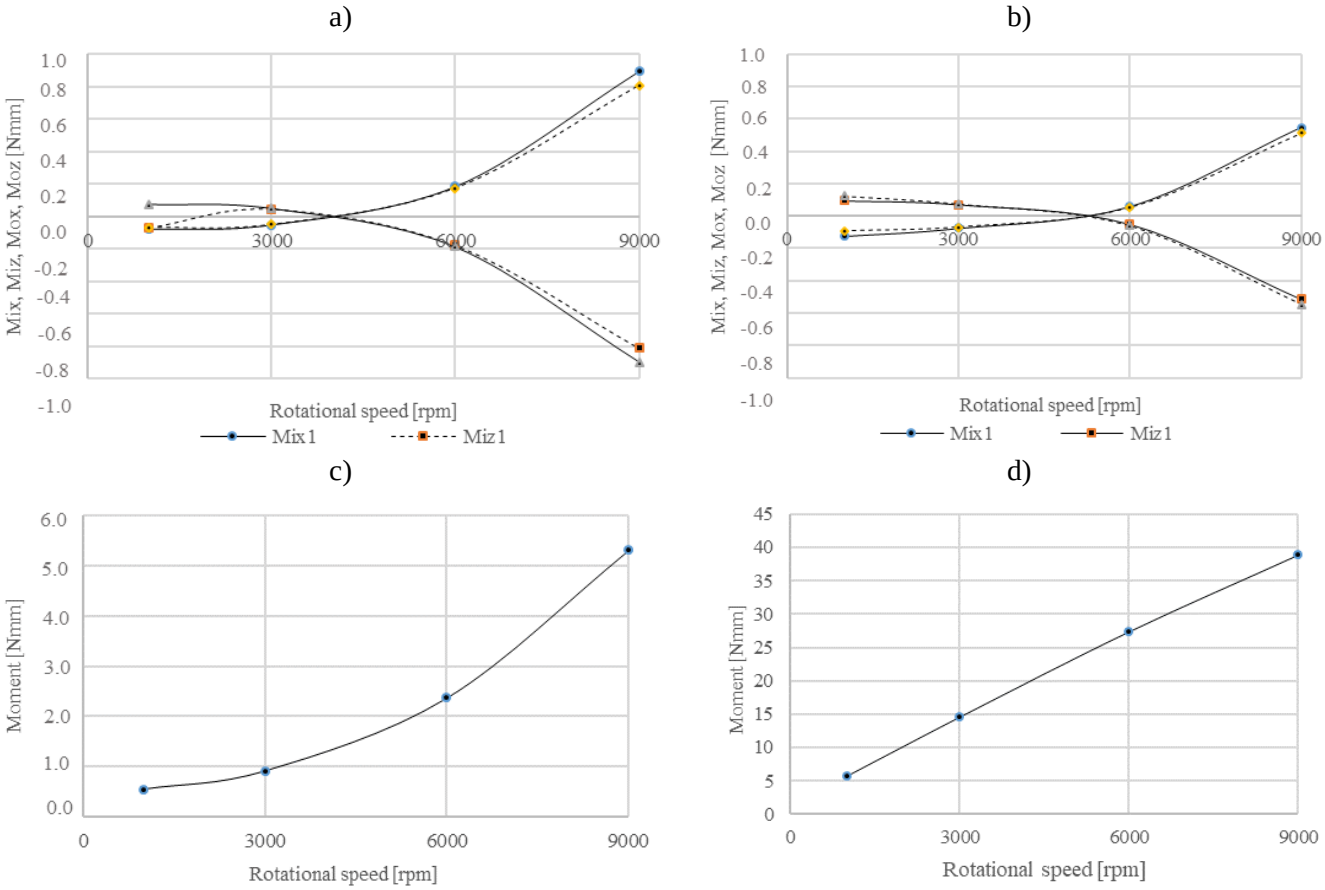

Fig. 14. Impact of rotational speed on: a), b) moments of force between the ball and raceways in the X and Z directions, c), d) moment of force between the body of the test stand and the torque sensor: a), c) without taking into account thermal effects, b), d) taking into account thermal effects

6. EXPERIMENTAL RESEARCH

As already mentioned, the object of the simulation tests was the test stand for measuring the resistance to motion of rolling bearings, which was built at the Department of Mechanical Engineering of the Silesian University of Technology (Fig. 1a). It enables stepless speed adjustment up to 18000 rpm and stepless adjustment of the preload of the bearings up to 1000N. Torque sensor Kistler type 7292 allows you to measure the moment of resistance to motion of bearings and the axial force sensor Kistler type 9102A allows you to measure the initial preload of the bearings. Temperature sensors (thermocouples type Pt-100), are glued to the outer rings of the bearings, while the temperature of the inner ring is measured with the use of an OptisCtLaser pyrometer. Moreover, a Vigo-Cam V50 thermal imaging camera was used to measure the temperatures of the test stand body.

Fig. 15 shows an example comparison of the temperature courses obtained from the simulation tests (*Tiv-var* and *Tov-var*) and from the experimental tests (*To Exp* and *Ti Exp*) for the speed of 6000 rpm. The time courses of temperatures from experimental and simulation studies measured on the outer rings of *To Exp* and *Tov-var* seem to be quite consistent. The same cannot be said for the *Ti Exp* and *Tiv-var* temperatures. In this case, we can only speak of a qualitative similarity. The likely cause of the large differences between *Ti Exp* and *Tiv-var* is the temperature measurement method with a pyrometer. Pyrometric methods of temperature measurement require fine-tuning of the so-called the emissivity factor but a default value was adopted in the conducted tests. Fig. 15 also shows the area limited by the *Ti Exp* and *To Exp* temperatures obtained from the experimental tests, inside which the temperatures obtained from the simulation tests are mixed.

The average temperature *Taverage* obtained from the simulation tests differs from the extreme temperatures *To Exp* and *Ti Exp* obtained from the experimental tests by less than 10% (Fig. 15).

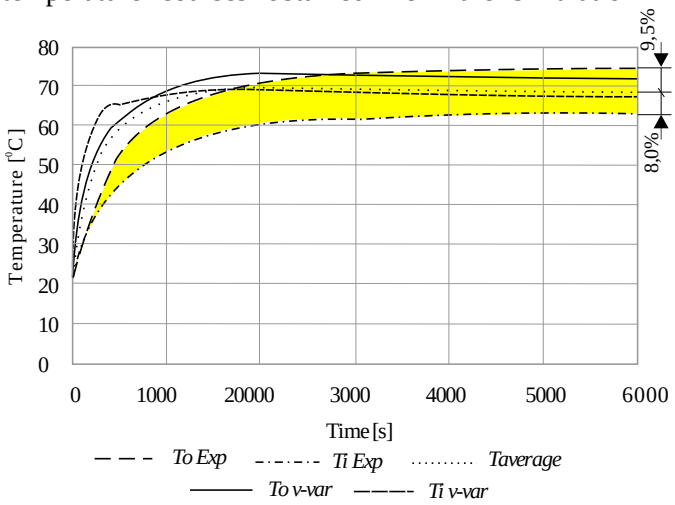

Fig. 15. An example of a comparison of temperature courses obtained from simulation tests (*Tiv-var* and *Tov-var*) and experimental tests (*To Exp* and *Ti Exp*) for a speed of 6000 rpm

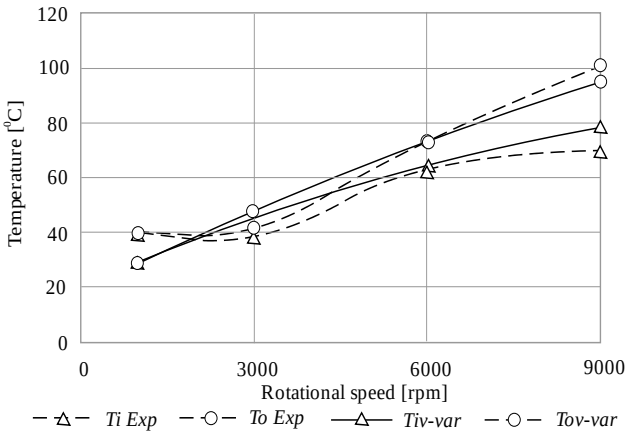

Fig. 16. Comparison of the influence of the bearing rotational speed on the temperatures obtained from the simulation tests (*Tiv-var* and *Tov-var*) and experimental (*To Exp* and *Ti Exp*)

Fig. 16 shows the influence of the bearing rotational speed on the temperatures obtained from the simulation tests (*Tiv-var* and *Tov-var*) and experimental tests (*To Exp* and *Ti Exp*). The comparison of these temperatures allows to draw a conclusion about the qualitative similarity, i.e. with the increase of speed, a higher temperature is observed, both on the outer and inner ring. On the other hand, quantitative compliance raises some doubts.

7. CONCLUSIONS

The article presents the results of simulation tests of the influence of heat generated in a bearing on its resistance to motion. So far, in the literature, there are results of analytical and simulation studies on the impact of dynamic loads due to such phenomena as centrifugal forces from spinning balls, moment due to gyroscopic phenomena or moment due to spin on resistance to motion. The literature also presents thermal effects in the form of power losses due to ball friction on raceways and viscous friction and their impact on thermal deformation of machine tool elements, e.g. machine tool spindles. However, there are no reports on how these power losses affect the resistance of the bearing itself. It can be assumed that the power loss in the bearing causes thermal deformation of the bearing elements, which in turn may change the clearance between the balls and raceways and, consequently, the resistance to motion.

Due to the complexity of kinematic and dynamic phenomena in the bearing, the author used the FEM simulation method to study resistance to motion. Analytical methods lead to complex mathematical models that require numerical, iterative solutions to them.

As a result of the research, the author showed:

- Obtaining the time course of temperatures in the bearing requires multiple iterative repetitions of the analyzes (Fig. 7).
- The time to reach the thermally steady state of the bearing can be as long as 1 hour (Fig. 7).
- Thermal deformation of bearing elements is many times greater than deformation caused by mechanical loads, e.g. centrifugal force from rotating balls or preload of bearings (Fig. 9 and Fig. 13b).
- The contact loads between the balls and raceways in the transient state can be many times greater than in the steady state (Fig. 10). This means, inter alia, the resistance to motion in the bearing in the transition state may be much greater than in the steady state.
- The steady state contact load modulus with thermal effects need not necessarily be greater than the contact load modulus disregarding thermal effects (Fig. 13g and Fig. 13h). On the other hand, the vectors of these loads do not necessarily have the same directions of action (Fig. 11).
- Moments due to contact forces in the transient state can be many times greater than in the steady state (Fig. 12). This means, inter alia, the resistance to motion in the bearing in the transition state may be much greater than in the steady state.

8. REFERENCES

1. Buchman, K.; Jungnickel, G., (1978). *Heat Transfer in Production Devices*, Publishing House of the Wroclaw University of Technology, Wroclaw, Poland.
2. Chwieduk, P., (2013). *MSc Thesis*, Silesian University of Technology, Gliwice, Poland.
3. Damian, I.; Paleu, V., (2013). *Mech. Test. Diagn. III 3*, pp. 18–24.
4. De-xing, Z.; Weifang, C.; Miaomiao, L., (2018). Appl. Therm. Eng., 131, 328–339.
5. Harris T.; Kotzalas M., (2007). *Rolling bearing analysis, Fifth edition Essential concepts of bearing technology*, Taylor&Francis Group 2007.
6. Holkup, T.; Cao, H.; Kolař, P.; Altintas, Y.; Zeleny, J., (2010). CIRP Ann. Manuf. Technol., 59, 365–368.
7. Kosmol J., (2021). Appl. Sci., 11, 6447, https://doi.org/10.3390/ app11146447.
8.Kosmol, J., (2021). Int. J. Mod. Manuf. Technol., 13, 73-83.
9. Kosmol, J., (2019). J. Theor. Appl. Mech., 57, 59–72.
10. Kosmol, J., (2018). J. Manuf. Sci. Eng., 140, 021002-1–021002-7.
11. Kosmol, J., (2016). *Determination of Motion Resistances in High. Speed Spindle Angular Bearings*, Silesian University of Technology Publisher, Gliwice, Poland.
12. Muszyński, M.; Kosmol, J.; Sokołowski, A., (2020). Int. J. Mod. Manuf. Technol., XII(1), 102–109.
13. Palmgren, A., (1951). *Rolling Bearing*, PWT, Warsaw, Poland.
14. Sum-Min, K.; Sun-Kuy, L., (2001). Int. J. Mach. Tools Manuf., 41(6), 809–831.
15.Wang, H.; Cai, Y.; Wang, H., (2017). Mech. Sci., 8, 277–288, doi:10.5194/ms-8-277-2017.
16. *Workbench User's Guide Ansys 2021R1*, (2021). Available online: https://www.coursehero.com/ file/70968250/Workbench-Users-Guide.pdf (accessed on 9 January 2021).
17. Zivkovic, A.; Zeljkovic, M.; Mladenovic, C.; Tabakovic, S.. (2018). Therm. Sci., doi:10.2298/TSCI180129118Z.
18. Zverev, I.A.; Eun, I.; Chung, W. J. ; Lee, Ch. M., (2003). KSME International Journal, pp. 668-678.

Received: May 30, 2022 / Accepted: December 15, 2022 / Paper available online: December 20, 2022 © International Journal of Modern Manufacturing Technologies